Epitaxial growth and magnetic properties of Mn_5Ge_3/Ge and $Mn_5Ge_3C_x$/Ge heterostructures for spintronic applications

Vinh Le Thanh, Aurélie Spiesser, Minh-Tuan Dau, Sion F Olive-Mendez, Lisa A Michez and Matthieu Petit.

Abstract

The development of active spintronic devices, such as spin-transistors and spin-diodes, calls for new materials that are able to efficiently inject the spin-polarized current into group-IV semiconductors (Ge and Si). In this paper we review recent achievements of the synthesis and the magnetic properties of Mn_5Ge_3/Ge and carbon-doped Mn_5Ge_3/Ge heterostructures. We show that high crystalline quality and threading-dislocation free Mn_5Ge_3 films can be epitaxially grown on Ge(111) substrates despite the existence of a misfit as high as 3.7% between two materials. We have investigated the effect of carbon doping in epitaxial Mn_5Ge_3 films and show that incorporation of carbon into interstitial sites of Mn_5Ge_3 can allow not only enhancement of the magnetic properties but also an increase of the thermal stability of Mn_5Ge_3. Finally, toward the perspective to realize Ge/Mn_5Ge_3/Ge multilayers for spintronic applications, we shall show how to use carbon to prevent Mn out-diffusion from Mn_5Ge_3 during Ge overgrowth on top of Mn_5Ge_3/Ge heterostructures. The above results open the route to develop spintronic devices based on $Mn_5Ge_3C_x$/Ge heterostructures using a Schottky contact without needing an oxide tunnel barrier at the interface.

Keywords: epitaxial MnGe compounds, spin injection, carbon-induced magnetic enhancement, carbon-induced thermal stability, group-IV semiconductors.

Introduction

Spintronics is an emerging field and one of the key requirements for its development rests on obtaining spin injectors, which not only have a high Curie temperature (TC) and a high spin polarization but also are compatible with the existing Si complementary metal–oxide semiconductor (CMOS) technology. Silicon- or germanium-based diluted ferromagnetic semiconductors (DMS) would be ideal candidates since they exhibit a natural impedance match to group-IV semiconductors. Unfortunately, $Si_{1-x}Mn_x$ alloys are not ferromagnetic and the use of $Ge_{1-x}Mn_x$ alloys would be hampered by their low T_C, which, in most cases, does not exceed 150K [1]. As a result, to make advances in applications much effort has been, in recent years, devoted to epitaxial ferromagnetic compounds that can be directly grown on Si and Ge substrates, such as Heusler alloys [2] or Mn_5Ge_3 [3–5]. Besides the fact that these compounds are fully compatible with the mainstream Si-based technology, they open the possibility of spin injection via tunnel effect through the Schottky barrier at the interface. Among these compounds, Mn_5Ge_3 is of particular interest since the bulk Mn_5Ge_3 compound is intermetallic, ferromagnetic at room temperature [6] and theoretical calculations have predicted an efficient spin injection along its c-axis [7], opening thus the possibility of spin injection without an external applied magnetic field, i.e. in remanent magnetic states. In addition, a spin polarization up to 42% has been demonstrated from Andreev reflection [8].

However, the Mn_5Ge_3 compound exhibits some drawbacks that need to be overcome for device applications: (i) firstly, according to the Ge-Mn bulk phase diagram, there are four phases at standard temperature and pressure conditions: Mn_3Ge,

Mn_5Ge_2, Mn_5Ge_3 and $Mn_{11}Ge_8$ [6, 9]. The first two phases are ferrimagnetic, Mn_5Ge_3 is the unique ferromagnetic phase and $Mn_{11}Ge_8$ is antiferromagnetic. Thus, starting from a system consisting of a thin Mn layer deposited on a Ge substrate, when thermal annealing is carried out to activate Ge/Mn interdiffusion, the most stable phase, which should be formed at high annealing temperatures, is the antiferromagnetic $Mn_{11}Ge_8$, having the highest Ge concentration. However, Mn_5Ge_3 is a unique phase, which has a hexagonal structure similar to a threefold symmetry of the (111) plane of the Ge; it can be then possible to be stabilized on Ge(111) by epitaxial effect. (ii) Secondly, the Curie temperature of Mn_5Ge_3 is only limited at room temperature (~296 K) while for device applications it is desirable that spin injectors have a magnetic order well above room temperature. Here, we shall show that incorporation of carbon atoms in interstitial sites of the Mn_5Ge_3 lattice greatly enhance the magnetic ordering of Mn_5Ge_3 films. Another important feature of a material for device applications is its thermal stability. Indeed, the thermal stability is a critical parameter for the integration of Mn_5Ge_3 into CMOS technology. In general, materials must remain stable up to temperatures higher than 700 °C since in the device fabrication process, numerous thermal anneals are needed, in particular after dopant implantation. We have then investigated the stability of Mn_5Ge_3 and carbon-doped Mn_5Ge_3 layers during post-grown thermal annealing, (iii) Thirdly, we have recently shown that the Mn segregation is a central problem that needs to be handled in order to get high-quality Ge/Mn_5Ge_3/Ge stacked layers [10, 11], which are the basis for numerous applications such as spin valves or the giant magnetoresistance effect. We shall summarize here the use of carbon to suppress the Mn segregation during Ge overgrowth on top of Mn_5Ge_3/Ge heterostructures.

Experimental

Mn_5Ge_3 and $Mn_5Ge_3C_x$ films were grown in a standard molecular-beam epitaxial (MBE) system with a base pressure better than $3x10^{-10}$ mbar. The growth system is equipped with a reflection high-energy electron diffraction (RHEED) to monitor the film growth mode and an Auger spectroscopy to control the film chemical composition. Mn_5Ge_3 and $Mn_5Ge_3C_x$ were grown on Ge(111) substrates using the solid phase epitaxial (SPE) technique, which consists of Mn deposition or co-deposition of Mn and C at room temperature followed by thermal annealing at temperature of ~450 °C to activate interdiffusion and phase nucleation. Mn and Ge evaporations were carried out using standard effusion cells; the Mn flux, measured with a quartz-crystal microbalance, is ~2 nm min^{-1} and the Ge flux, deduced from RHEED intensity oscillations, is in the range of ~2–5 nm min^{-1}. Carbon evaporation was carried out using a sublimation source of high-purity pyrolytic graphite, the carbon concentration was estimated by using the change of Si(001) surface reconstructions from (2x1) to c(4x4) upon adsorption of a carbon submonolayer.

The cleaning of the Ge surfaces was carried out using the HF-last dip method similar to that used for the Si substrate [12] to minimize native oxide. The second step was an in situ thermal cleaning, which consists of outgassing the sample for several hours at 450 °C followed by flash annealing ~650 °C to remove the residual Ge surface oxide, which can be formed during sample transfer into a high vacuum. After this step, the Ge(111) surface generally exhibits a relatively well-developed c(2x4) reconstruction.

Structural characterizations of grown films were performed by means of high-resolution transmission electron microscopy (HR-TEM) using a JEOL 3010 microscope operating at 300 kV with a spatial resolution of 1.7 Å. Complementary structural characterizations were carried by means of x-ray diffraction (XRD) using a diffractometer (Philips X'pert MPD) equipped with a copper target for Cu-$K_{\alpha 1}$ radiation (λ = 1.540 59 Å). The angular resolution is ~0.01°.

The magnetic properties of the films were probed using a superconducting quantum interference device (SQUID) magnetometer with a magnetic field applied both in-plane and out-of-plane of the sample surface. The diamagnetic contribution arising from Ge was subtracted, leaving only the magnetic signal coming from Mn_5Ge_3 and $Mn_5Ge_3C_x$ films.

Results and discussion

This section will be divided into four subsections in which we present results concerning the epitaxial growth as well as the magnetic properties of Mn_5Ge_3 grown on Ge(111) substrates, the effect of carbon doping on the magnetic properties and thermal stability of Mn_5Ge_3 films and finally the Mn segregation and the method to suppress it. Epitaxial growth and magnetic anisotropy of Mn_5Ge_3/Ge(111) heterostructures:

In a conventional MBE, the growth of an epitaxial film can proceed via two main techniques: solid phase epitaxy (SPE) and reactive deposition epitaxy (RDE). The SPE consists of deposition or co-deposition of materials at room temperature, then followed by thermal anneals in order to activate diffusion and/or interdiffusion of species. This method involves therefore two successive processes: first, diffusion and/or interdiffusion

occur and then phase nucleation takes place, which starts from the interface. In RDE, materials are deposited or co-deposited on the substrate surface, which is kept at high temperatures. Depending on the substrate temperature, different phases can be formed but the phase nucleation is the main process, which occurs at the growing surface as the growth advances. Since Mn_5Ge_3 is not the most stable phase and has a hexagonal structure similar to that of Ge(111), the SPE technique, which allows Mn_5Ge_3 films to easily adopt the substrate symmetry from the interface, naturally appears more appropriate than the RDE to form epitaxial Mn_5Ge_3 films. Indeed, our unpublished results show that when using the RDE technique, a fraction of the $Mn_{11}Ge_8$ phase may coexist with Mn_5Ge_3. Starting from a thin Mn film deposited on a Ge(111) substrate at room temperature, we have shown that Mn_5Ge_3 is the unique epitaxial phase that can be formed upon annealing in the temperature range of 430–600 °C [4, 5]. The $Mn_{11}Ge_8$ phase, which is the richest in Ge, is formed only when annealing at temperatures higher than 650 °C [13]. Below 650 °C, the coexistence of two phases, Mn_5Ge_3 and $Mn_{11}Ge_8$, may be observed, but only when the initial Mn film is thick enough (>210 nm) [14] or when films are grown on an amorphous oxide substrate [15].

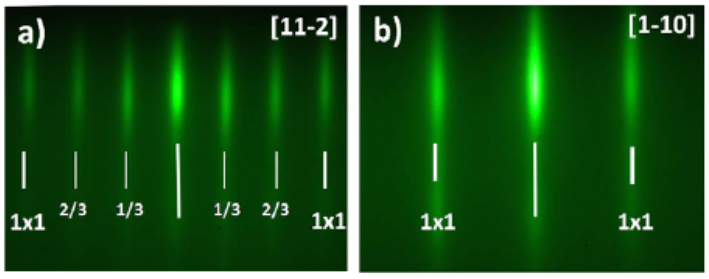

Figure 1. Typical RHEED patterns taken along (a): the [11–2] and (b): [1–10] azimuth of an epitaxial Mn_5Ge_3 film. Additional 1/3 and 2/3 ordered streaks are observed along the [11–2] azimuth, defining a RHEED $(\sqrt{3} \times \sqrt{3})R30^\circ$ surface reconstruction; (1×1) indicates bulk-like streaks.

Figures 1(a) and (b) show typical RHEED patterns observed during epitaxial growth of Mn_5Ge_3 on Ge(111). Stating from a clean (2x4) reconstructed Ge(111) surface, RHEED patterns indicate that Mn_5Ge_3 films display a hexagonal symmetry similar to that of the substrate. By combining RHEED patterns with TEM backside electron diffraction analysis, it is found that the hexagonal basal (0001) plane of Mn_5Ge_3 is parallel to the (111) plane of Ge. The epitaxial relationship has following form:

$$Mn_5Ge_3(0001) \parallel Ge(111)$$
$$\text{with } [110]_{Mn5Ge3} \parallel [1-10]_{Ge}.$$

The Mn5Ge3 surface is characterized by a RHEED ($\sqrt{3}$x$\sqrt{3}$)R30° reconstruction, defined by the observation of 1x1 streaks along the [1–10] azimuth and additional 1/3- and 2/3-ordered streaks along the [11–2] azimuth. Interestingly, long streaks are observed in RHEED patterns for film thicknesses in the range between some nm up to about 160 nm, indicating that the film surface is highly smooth.

A high-resolution TEM image taken near the interface region of a 25 nm thick Mn_5Ge_3 film is shown in figure 2(a). The image clearly reveals atomic lattice planes of both the Ge substrate and Mn_5Ge_3 film. The film is highly ordered and the interface is atomically abrupt, no intermixing is observed. Of particular interest, with a misfit as high as 3.7%, almost no threading dislocations can be detected. XRD measurements of the corresponding sample are displayed in figure 2(b). In addition to the (hhh) reflections of the Ge(111) substrate [(111) and (333) reflections], only (002) and (004) hkl reflections of Mn_5Ge_3 are observed, thus confirming the epitaxial relationship of the film, being Mn_5Ge_3(001) || Ge(111).

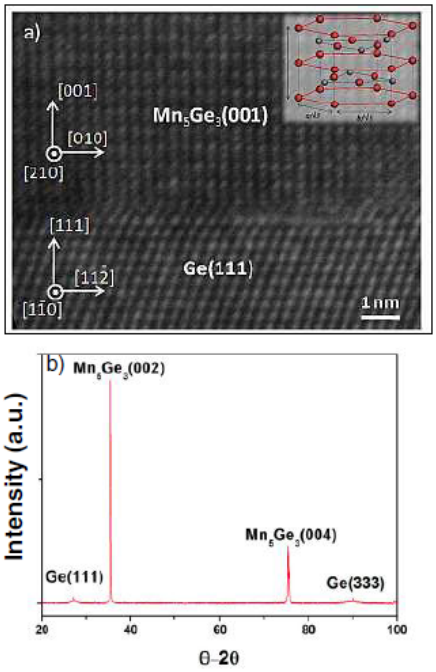

Figure 2. (a) Atomically resolved cross-sectional TEM image taken near the interface region of a 25 nm thick Mn_5Ge_3 film grown on Ge(111). Shown in inset is a side view of a schematic hexagonal structure of a Mn_5Ge_3 cell; (b) XRD θ–2θ scan of the corresponding sample.

A systematic study of the magnetic properties of Mn_5Ge_3 has been carried out as a function of the film thickness ranging from 5 up to 160 nm. We show in figure 3 some representative hysteresis (M–H) loops measured with in-plane and out-of-plane magnetic field. Insets represent a zoom around the positive saturation field of the out-of-plane configuration. Parallel and perpendicular configurations for thick samples lead apparently to similar magnetic reversal; this is surprising since we expect an easy magnetization axis along the c-axis, which is perpendicular to the sample plane. However, in-plane M–H curves reveal a steady change in the magnetic behavior: for samples thinner than 10 nm, the hysteresis loop exhibits a square shape that unambiguously indicates that the magnetization easy axis lies in-plane; for thicker

samples, the M–H curves become increasingly canted as the saturation field increases with thickness but a hysteresis is still visible around zero field.

In the out-of plane configuration, at first sight, the hysteresis loops appear similar throughout the range of the studied thicknesses: little hysteresis is present and the saturation fields are higher than the ones observed in the parallel configuration. However, when looking at the variation of the perpendicular saturation field versus the film thickness, two regimes can clearly be distinguished: firstly, below thicknesses of about 20 nm, the perpendicular saturation field increases rapidly with the film thickness; secondly, above this thickness, it is independent of the film thickness and fluctuates around 10 000±1000 Oe.

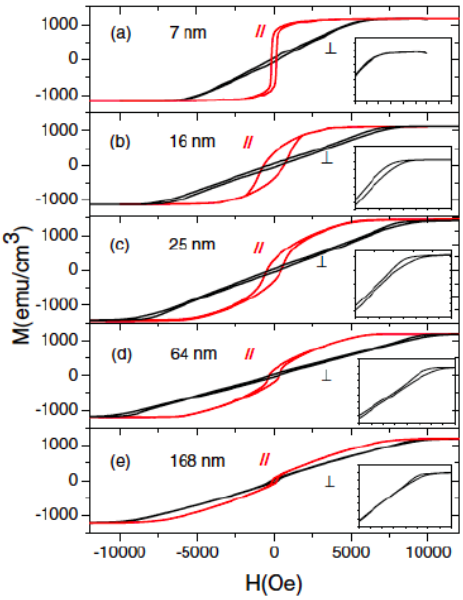

Figure 3. Magnetic hysteresis curves with the external magnetic field applied in the sample plane and perpendicular to it for different thicknesses of Mn_5Ge_3 films: (a) 7 nm; (b) 16 nm; (c) 25 nm; (d) 66 nm; (e) 168 nm. Insets zoom in the positive field branch (from 4000 to 12 000 Oe) of the perpendicular configuration. All the measurements have been done at 15 K.

More importantly, the general shape of the hysteresis curves changes. Above a threshold thickness, a singularity in all the out-of-plane M–H curves appears around the saturation field as demonstrated in the inset of figure 3(c) for a 25 nm thick sample. By describing the M–H curve from positive saturation to lower field values, a characteristic opening of the hysteresis loop appears around the saturation field over a narrow range of fields. As the field decreases, the two M–H branches return to similar field dependence and this singularity disappears. This feature is not present in hysteresis loops of layers thinner than 10 nm where the magnetization rises linearly with the applied field and almost reversibly. In [16], we have provided a detailed analysis of the evolution of Mn_5Ge_3 magnetic properties versus the film thickness and show that the reorientation of the magnetization from in-plane to out-of-plane occurs for a film thickness lying between 10 and 25 nm. This result is strongly supported by theoretical calculations based on an improved version of Kittel's model to retranscribe the magnetic behavior of domains in uniaxial thin films. Of particular interest, the size of magnetic domains in Mn_5Ge_3 is shown to be considerably smaller than the one in any other known magnetic system and it can be in addition tailored by the film thickness.

Enhancement of the Curie temperature in carbon-doped Mn_5Ge_3 films: The enhancement of the magnetic properties of polycrystalline Mn_5Ge_3 films induced by carbon doping was first demonstrated by Gajdzik et al [17] using sputtering deposition technique. Later, Slipukhina et al [18] calculated exchange-coupling constants in Mn_5Ge_3C alloys and showed that the enhanced ferromagnetic stability in the alloy mainly results from interactions between Mn atoms mediated by carbon incorporated in octahedral voids of the hexagonal Mn_5Ge_3 cell. To incorporate as high as possible

carbon atoms into interstitial sites of the Mn_5Ge_3 cell, we have implemented the SPE technique in order to promote carbon diffusion. Indeed, since the atomic radius of carbon is almost twice as small as that of Mn and Ge, it follows that in a growth process where carbon atoms can diffuse, it becomes easier for them to be incorporated in the interstitial site.

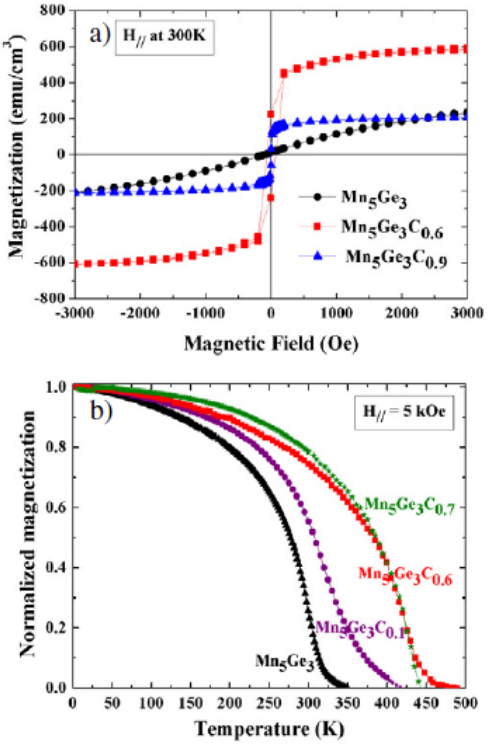

Figure 4. (a) Hysteresis loops of different carbon-doped Mn_5Ge_3 films measured at 300 K with magnetic field applied in the film plane; (b) evolution of normalized magnetization as a function of the temperature for various values of x in $Mn_5Ge_3C_x$ films.

The effects of the carbon concentration on the magnetic properties of $Mn_5Ge_3C_x$ films are depicted in figure 4. Figure 4(a) displays hysteresis loops of C-free Mn_5Ge_3 and $Mn_5Ge_3C_x$ films with various carbon concentrations, measured by SQUID at 300K with a magnetic field of 0.5 T applied in the film plane. At 300K the hysteresis loops of the C-free Mn_5Ge_3 film exhibit a paramagnetic character, as being expected because C-

free Mn_5Ge_3 is ferromagnetic only up to 296 K. For C-doped Mn_5Ge_3, hysteresis loops measured at 300K clearly indicate that the materials are ferromagnetic within the whole range of the carbon concentration. It is worth noting that while the measurements at 300K confirm that at x = 0.9 the film remains ferromagnetic, the hysteresis loops measured at 5K (not shown here) display an oblate shape and show a great reduction of net magnetization [19, 20]. The temperature dependence of normalized magnetization of $Mn_5Ge_3C_x$ with various carbon concentrations is presented in figure 4(b).

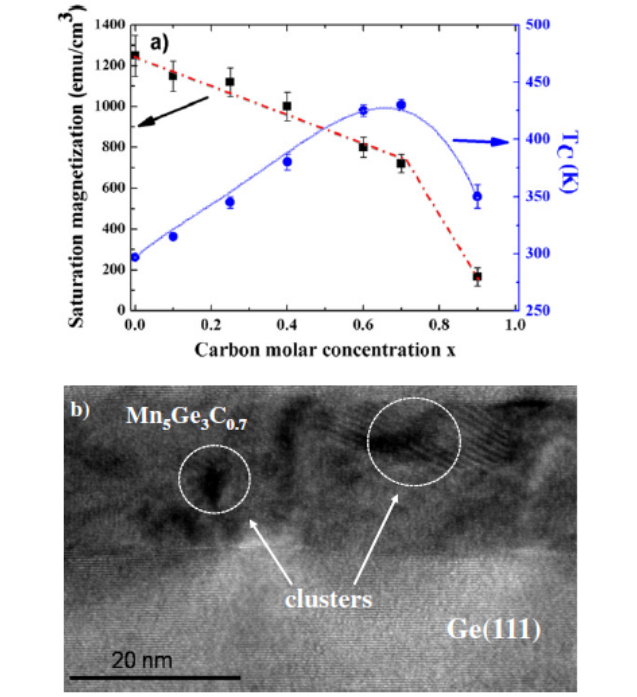

Figure 5. (a) Evolution of saturation magnetization M_S (left axis) and T_C (right axis) versus the carbon concentration. Note that dotted lines for M_S evolution and solid lines for carbon dependence of T_C serve as a guide to the eye; (b) typical cross-sectional TEM image of a $Mn_5Ge_3C_{0.7}$ film, which reveals the formation of clusters inside the film.

For comparison, we also show a curve of a C-free Mn_5Ge_3 film of the same thickness. The figure clearly indicates that addition of carbon strongly enhances

magnetization of Mn_5Ge_3 and such an enhancement continuously increases with the carbon concentration up to 0.7. The T_C, measured at the inflection point of the curve M versus T , reaches a value of ~430K for x = 0.6 and 0.7. We note that if we determine the T_C from the extrapolation of the M(T) data to M(TC) = 0, the T_C of the $Mn_5Ge_3C_{0.6}$ curve gives a value up to 460 K.

We report in figure 5(a) the variations of T_C and of magnetization at saturation (MS) as a function of the carbon concentration. The variation of T_C with x occurs in two distinct regions: T_C first linearly increases with x up to 0.6–0.7, then falls for larger values of x. Note that this behavior is different from that previously reported for polycrystalline films [17]. The evolution of MS, measured at 5 K, is well correlated with the T_C variation. Saturation magnetization is found to linearly decrease with x and at x = 0.6–0.7, an abrupt change in the slope is observed. We note that in transition metals and their alloys, it is generally observed that magnetization at saturation increases when increasing the Curie temperature. However, as previously mentioned, in $Mn_5Ge_3C_x$ the ferromagnetic enhancement results from Mn_{II}–Mn_{II} interactions mediated by carbon atoms inserted into the voids of Mn octahedra of the hexagonal structure. Consequently, carbon incorporation into Mn_5Ge_3 changes the 3d states of neighboring Mn atoms and the hybridization between the C 2p andMn_{II} 3d states leads to a decrease of magnetization of saturation as well as magnetic moment on Mn_{II}.

These results indicate that the saturation concentration of carbon, which can be inserted into interstitial sites of the Mn_5Ge_3 lattice is around x ~0.6–0.7. From measurements of the magnetic moment at saturation and the film thickness deduced from TEM images, an average saturated Mn moment of ~1.9μ_B/Mn is deduced for x =

0.7. This value is close to the one obtained in C-implanted films [21] and with theoretical calculations [18], but deviates from the values obtained for the sputtered films, where the highest moment of 1.1μ_B/Mn was observed [17].

To understand the decrease of T_C for x > 0.7, we show in figure 5(b) a typical TEM image of a sample corresponding to x = 0.7. It is worth noting that for x 6 0.6, TEM images of carbon-doped Mn_5Ge_3Cx alloys are similar to that of carbon-free Mn_5Ge_3 shown in figure 2(a) in which the film is of high crystalline quality and the interface is atomically smooth. The presence of clusters or precipitates in the grown film can be clearly seen from this image. In order to identify the nature of clusters that are formed for x > 0.7, thermodynamic calculations of the formation energy of the carbon defects in Mn_5Ge_3 have shown that the $Mn_5Ge_3C_{0.5}$ alloy is a stable ternary alloy and additional carbon atoms cannot be inserted into interstitial sites, but will rather form clusters of manganese carbides (MnC) [19]. Two main phases, Mn_7C_3 and/or Mn_5C_2, appear to be energetically favorable when the carbon concentration becomes higher than 0.5.

Thermal stability of Mn_5Ge_3 and carbon-doped Mn_5Ge_3 films: The thermal stability of an active material is one of the crucial parameters that need to be determined and controlled for its integration in the device fabrication process. We display in figure 6(a) the change of magnetization of a 100 nm thick Mn_5Ge_3 film after annealing at 650 °C. Before annealing, hysteresis loops of Mn_5Ge_3 exhibit ferromagnetic behavior as expected. The magnetization at saturation (MS) is ~1300 emu cm^{-3} and the average magnetic moment per Mn atom (μ_s) is ~3.2μ_B. These values are close to those reported in literature for thin films [3, 4] and bulk materials [22]. After

annealing at 650 °C, the magnetization at saturation (MS) is found to decrease down to 6 emu cm^{-3} and the remanent magnetization reduces from 125 to 1 emu cm^{-3}.

To get a better insight into the origin of the above drastic change in magnetic properties of Mn_5Ge_3 upon annealing, we present in figure 6(b) a comparison of magnetization versus temperature before and after annealing. The as-grown sample clearly displays a ferromagnetic behavior characteristic of Mn_5Ge_3; the TC, measured at the inflection point of the M(T) curve, is ~296 K. After annealing at 650 °C, the M(T) curve reveals two distinct transitions: an antiferromagnetic/ferromagnetic transition at ~150K and a ferromagnetic/paramagnetic transition at ~270 K. Such a magnetic signature can be unambiguously attributed to the antiferromagnetic $Mn_{11}Ge_8$ compound [23].

Thus, the above results confirm that Mn_5Ge_3, which is not a stable phase, can be stabilized on Ge(111) by epitaxy due to the similarity of its hexagonal structure compared to that of Ge(111). As defined by thermodynamics, post-thermal annealing of grown films should bring the system toward a more equilibrium state, i.e. to the formation of $Mn_{11}Ge_8$, which is the most stable phase in the Mn/Ge phase diagram. Since the Ge concentration in Mn11Ge8 is of ~42% compared to ~37.5% in Mn_5Ge_3, such a phase transformation should require a long-range diffusion of Ge from the substrate.

Regarding the thermal stability of C-doped Mn_5Ge_3, as mentioned above, doping Mn_5Ge_3 with carbon allows increasing its T_C, and such an enhancement has been explained due to Mn_{II}–Mn_{II} interactions mediated by carbon atoms [18].

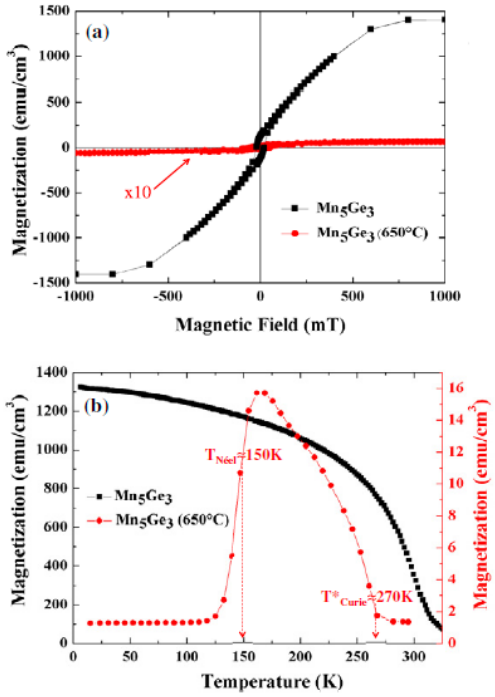

Figure 6. (a) Evolution of hysteresis loops of a 100 nm thick Mn_5Ge_3 film before and after annealing at 650 °C. Measurements were carried out at 15 K with magnetic field applied in the film plane; (b) temperature dependence of magnetization of the corresponding sample before (left axis) and after annealing at 650 °C (right axis). Measurements were performed with a magnetic field of 500 mT applied in the film plane.

Figure 7(a) shows the magnetization enhancement induced by carbon doping (black curve corresponding to Mn_5Ge_3 and green one to $Mn_5Ge_3C_{0.6}$). It can be seen that the $Mn_5Ge_3C_{0.6}$ curve exhibits a T_C up to ~460 K, compared to 296K of Mn_5Ge_3. Figure 7(b) shows the evolution of hysteresis loops of the $Mn_5Ge_3C_{0.6}$ film upon annealing at 750 and 850 °C. The most interesting feature is that the carbon-doped Mn_5Ge_3 layers remain ferromagnetic even after annealing at 850 °C. The hysteresis loops conserve its squareness up to 750 °C, beyond which an increase of the coercive field occurs, which can be probably attributed to the formation of point defects due to high annealing temperatures. Thus, the above results provide evidence that inserting carbon into interstitial sites of Mn_5Ge_3 allows great improvement in its thermal stability.

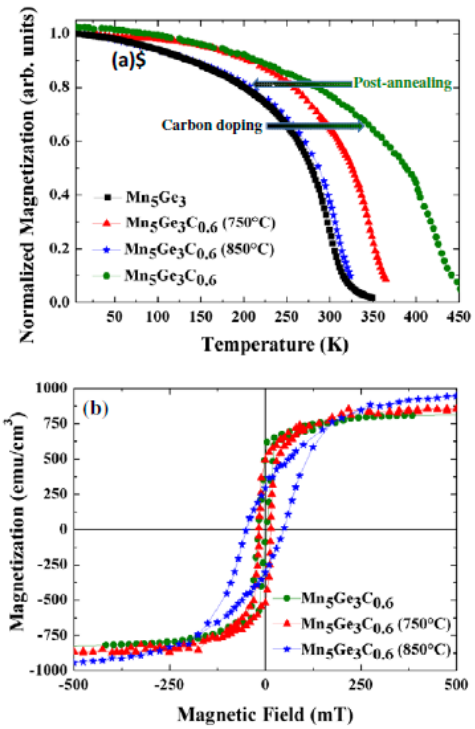

Figure 7. (a) Temperature dependence of magnetization illustrating a reversible evolution of T_C of a 20 nm thick Mn_5Ge_3 film upon carbon doping and annealing for a film with a carbon concentration of 0.6. Measurements were performed with a magnetic field of 500 mT applied in the film plane; (b) evolution of hysteresis loops of a 20 nm thick $Mn_5Ge_3C_{0.6}$ film after annealing at 750 and 850 °C. Measurements were performed at 15 K with magnetic field applied in the film plane.

Another interesting feature that can be seen in figure 7(a) is a reversible transition of T_C upon carbon doping and annealing. Doping Mn_5Ge_3 with carbon allows enhancing T_C from 296 up to 460 K, which is found to decrease down to 350 and 307K when increasing the annealing temperature to 750 °C (red curve) and 850 °C (blue curve), respectively. Other magnetic parameters, such as M_{sat} and μ_s, also exhibit a similar reversible transition. For example, in Mn_5Ge_3 the measured value of μ_s is ~3.2μ_B, which is found to decrease down to ~1.9μ_B in $Mn_5Ge_3C_{0.6}$. Upon annealing, μ_s progressively increases with increasing temperature and almost reaches the initial value of ~3.2μ_B after annealing at 850 °C. Such results imply that carbon atoms, which have

been incorporated into interstitial sites of Mn_5Ge_3, are progressively extracted during annealing.

Mn segregation and its suppression induced by carbon adsorption: In numerous spintronic applications, such as spin valves or giant magnetoresistance (GMR) superlattices, high-quality Ge overgrowth on top of Mn_5Ge_3 films is needed. One of the difficulties inhibiting the realization of Ge/Mn_5Ge_3 heterostructures with abrupt interfaces would be probably the Mn segregation. As we have mentioned above, since epitaxial Mn_5Ge_3 films give rise to additional RHEED streaks compared to the Ge surface, we have used RHEED to monitor in real time and in situ, the Mn segregation process by measuring the intensity evolution of these additional streaks versus the Ge deposition time or the thickness [10]. A typical result of intensity measurements of a 2/3 streak at three different substrate temperatures, 200, 450 and 550 °C, is reported in figure 8.

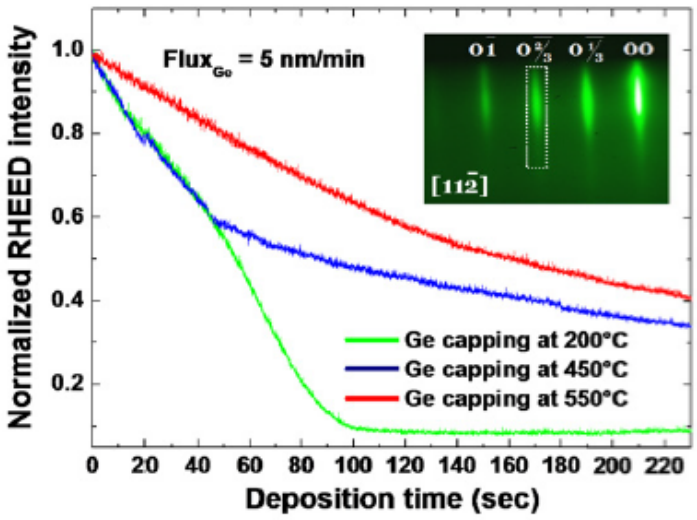

Figure 8. The evolution of RHEED intensity recorded during Ge deposition at 200, 450 and 550 °C. Intensity measurements were taken in the region surrounding a 2/3 ordered streak (dotted line) along the [11–2] azimuth.

Two distinct behaviors regarding the scale of the deposition time of the Ge overlayers are clearly observed. At 200 °C, the intensity of the 2/3 streak vanishes at around 95 s, while at 450 and 550 °C it continues to a much higher deposition time and completely disappears only after a Ge deposition of more than 800 s. The corresponding Ge thickness is ~8 nm at 200 °C and it is larger than 70 nm at 450 and 550 °C. It is worth noting that the surface segregation of an element during the growth of heterostructures or multilayers has been observed in many systems, including III–V materials [24] or Si on SiGe [25]. However, at usual growth temperatures (~600 °C), the segregation length does not, in general, exceed a dozen nanometers.

To understand the different behavior of Ge overgrowth observed at low and high temperatures as described above, we have systematically performed TEM analyses of samples grown at 450 and 550 °C. Figure 9(a) displays a typical cross-sectional TEM image taken after the deposition of 60 nm of Ge at 450 °C. To see the evolution of different layers in the final structure more clearly, we show, in figure 9(b), a schema of the designed sample in which the thickness of each layer is indicated.

Contrary to the designed structure, the TEM image reveals that the sample surface is terminated by a Mn_5Ge_3 layer and no trace of Ge overlayers is detectable. Indeed, the observation in this TEM image of well-defined atomic rows, all being perpendicularly aligned to the interface, can be unambiguously attributed the hexagonal (0001) plane of Mn_5Ge_3, which is parallel to the (111) plane of Ge [4, 19]. Thus, TEM analyses indicate that upon Ge deposition at 450 °C, it is not a Ge layer which is progressively formed on the surface as expected but the deposited Ge reacts with Mn to

form the Mn_5Ge_3 compound. Interestingly, the Mn_5Ge_3 surface layer has a thickness of ~20 nm, a value slightly thinner than the initial thickness of the starting Mn_5Ge_3 layer.

It can also be seen that the whole Mn_5Ge_3 layer continuously floats on the surface as the Ge deposition progresses, leaving behind newly formed Ge layers.

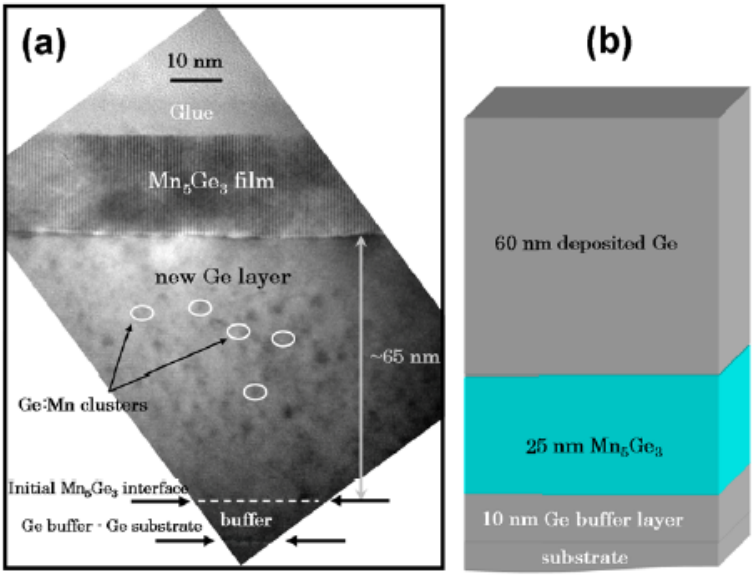

Figure 9. (a) Cross-sectional TEM image of a sample after deposition of a 60 nm thick Ge layer at 450 °C. The dotted line indicates the initial interface between the Ge buffer layers and the Mn_5Ge_3 film. The presence of Ge:Mn precipitates or clusters in the Ge substrate is indicated; (b) schema illustrating the corresponding designed structure. Note that to produce a 25 nm thick Mn_5Ge_3 film by the SPE technique, a Mn film with a thickness of about 15 nm was deposited.

In other words, the Mn_5Ge_3 film behaves here as a surfactant, which floats upwards the growing surface, similar to the case of monolayer-thick Mn adsorbed on Ge(001) [26]. An interesting feature that can be seen from the image is the presence of Mn-rich clusters embedded inside the lower Ge layers. We notice that in standard Mn_5Ge_3/Ge heterostructures, Mn–Ge clusters are never observed in the Ge substrate after Mn_5Ge_3 growth at 450 °C [4, 5, 16] or even after post-annealing up to 650 °C [13].

The formation of such clusters can be attributed to the fact that in the case of the Ge deposition on Mn_5Ge_3 at 450 °C, the initial epitaxial Mn_5Ge_3 film, because of its metastable state, is destabilized even at its interface with the substrate, which is 25 nm from the surface. Consequently a part of Mn is detached around the interface region and diffuses into the substrate, resulting in the formation of Mn-rich clusters. This explains why the thickness of the final floating Mn_5Ge_3 film is slightly thinner than the initial one.

To prevent out-diffusion of an element, it is common to use a diffusion barrier, and materials must be not only nonreactive but also are able to strongly adhere to adjacent materials. In electronic or memory devices, multilayers of metals, WN_2, RuTiN or RuTiO, are usually used to prevent out-diffusion of dopants (B and P) or oxidation of devices [27–29]. Such materials are, however, difficult to insert in a heterostructure where epitaxial growth is needed. Since any segregation process should involve a rapid and long-range diffusion of elements, which, in general, occurs via interstitial diffusion, our approach consists of filling in the interstitial sites of Mn_5Ge_3 prior to Ge deposition. To experiment with the filling, we choose carbon for its small atomic radius. The principle of experiments is described in figure 10(a), consisting of depositing some carbon MLs on Mn_5Ge_3 prior to Ge growth.

The amount of adsorbed carbon should be an important parameter, and it was chosen according to the change in RHEED patterns.

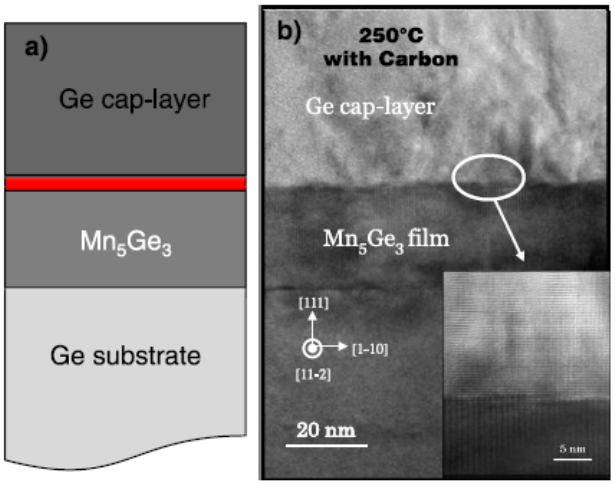

Figure 10. (a) Schema explaining the different growth steps of $Ge/Mn_5Ge_3/Ge$ structures with carbon adsorption (red) on top of Mn_5Ge_3 prior to the deposition of Ge overlayer; (b) cross-sectional TEM image of a ~50 nm thick Ge film deposited on Mn_5Ge_3 with a pre-adsorption of 4 ML of carbon on the top. The temperature of carbon and Ge depositions is 250 °C. Shown in the inset is an atomically resolved TEM image of the interface region. The (111) plane of Ge overlayers is parallel to the hexagonal basal (0001) plane of Mn_5Ge_3.

Upon carbon adsorption, the √3 RHEED characteristic of Mn_5Ge_3 remains almost unchanged up to carbon coverage of 4 ML, beyond which a faint pattern is observed. Since we search a high filling degree of Mn_5Ge_3 interstitial sites, a carbon amount of 4 ML is then chosen. It is worth noting that carbon adsorption at room temperature or at 250 °C produces almost similar results. Figure 10(b) shows a typical structure of a sample containing 4 ML of carbon adsorbed at 250 °C.

Even if the Ge overlayers are far from perfect, the image clearly reveals that the Ge/Mn_5Ge_3 interface has become much smoother. A much smaller Mn segregation length is confirmed by RHEED analyses, which reveal that a *c*(2x4) reconstruction characteristic of a clean Ge(111) surface quickly appears only after deposition of

some Ge MLs. The improvement of Mn out-diffusion is also confirmed by Auger measurements, which reveal that Mn transitions, located at 537, 584 and 631 eV,

almost disappear after 3 nm thick Ge deposition while on C-free samples Mn signals persist for Ge thickness larger than 10 nm. Shown in the inset is an atomically resolved image of the interface region. Clearly, no Mn-rich clusters are present, and more importantly, well-ordered (111) planes of Ge overlayers are found to be perpendicular to the atomic rows produced by Mn arrangement along [0001] direction of the underneath Mn_5Ge_3. However, it is worth noting that when carbon adsorption on the Mn_5Ge_3 surface is carried out at temperatures > 450 °C, manganese carbides can be formed and the resulting Ge overlayer changes its orientation from (001) to (111), which has a higher surface energy [30].

Conclusion

To summarize, we have investigated the epitaxial growth of Mn_5Ge_3 and carbon-doped Mn_5Ge_3 films on Ge(111) and evidenced numerous features, which may render these materials of high potential for the development of spintronic devices compatible with group-IV semiconductors. High crystalline quality Mn_5Ge_3 films can be obtained despite the existence of a lattice mismatch as high as 3.7%. Of particular interest, the epitaxial Mn_5Ge_3 film is strain relaxed but displays an extremely low density of threading dislocations. This interesting feature can be attributed to a high value of the elastic modulus of Mn_5Ge_3, which is 110 GPa compared to 77.2 GPa for Ge, thus allowing Mn_5Ge_3 films to be easily elastically deformed on Ge. We have shown that Mn_5Ge_3 is not a stable phase but can be stabilized on Ge(111) thanks to the similarity of its crystal structure compared to that of Ge(111). Upon annealing at 650 °C, Mn_5Ge_3 transforms into the antiferromagnetic $Mn_{11}Ge_8$ phase. The reorientation of the magnetization in

Mn_5Ge_3 films from in-plane to out-of-plane is found to occur at film thicknesses lying between 10 and 25 nm, which are much smaller compared to other uniaxial thin films.

In an effort to insert as much carbon as possible into the octahedral voids of the hexagonal Mn_5Ge_3 lattice, we have implemented the solid phase epitaxy technique, which allowed us to insert carbon up to a saturation concentration of ~0.6–0.7. When the carbon concentration increases from 0 to the saturation value, the Curie temperature of the alloys is found to linearly increase with x, reaching a value as high as 460 K. When the carbon concentration is higher than the saturation value, the formation of manganese carbides becomes thermodynamically more favorable. Doping Mn_5Ge_3 with carbon also allows great enhancement of its thermal stability, the materials remain ferromagnetic up to a temperature as high as 850 °C. We have also shown that the realization of Ge/Mn_5Ge_3 multilayers is hampered by Mn segregation toward the Ge growing surface and adsorption of some monolayers of carbon on top of the Mn_5Ge_3 surface prior to Ge deposition allows great reduction of Mn segregation.

Acknowledgments

We specially thank P Pochet and colleagues in his group for thermodynamic calculations of the Curie temperature of $Mn_5Ge_3C_x$ compounds. We also thank R Hayn and F Virot for their theoretical work to explain the magnetic anisotropy in Mn_5Ge_3 films. The contributions of S Bertaina andMJamet in magnetic characterizations are greatly acknowledged.

References

[1] Park Y D, Hanbicki A T, Erwin S C, Hellberg C S, Sullivan J M, Mattson J E, Ambrose T F, Wilson A, Spanos G and Jonker B T 2002 Science 295 651

[2] Hamaya K, Itoh H, Nakatsuka O, Ueda K, Yamamoto K, Itakura M, Taniyama T, Ono T and Miyao M 2009 Phys. Rev. Lett. 102 137204

[3] Zeng C, Erwin S C, Feldman L C, Li A P, Jin R, Song Y, Thompson J R and Weitering H H 2003 Appl. Phys. Lett. 83 5002

[4] Olive-Mendez S F, Spiesser A, Michez L A, Le Thanh V, Glachant A, Derrien J, Devillers T, Barski A and Jamet M 2008 Thin Solid Films 517 191.

[5] Spiesser A, Olive-Mendez S F, Dau M-T, Michez L A, Watanabe A, Le Thanh V, Glachant A, Derrien J, Barski A and Jamet M 2010 Thin Solid Films 518 S113

[6] Massalki T B 1992 Binary Alloy Phase Diagrams vols 1 and 2, 2nd edn (Materials Park, OH: ASM International)

[7] Picozzi S, Continenza A and Freeman A J 2004 Phys. Rev. B 70 235205

[8] Panguluri R P, Zeng C, Weitering H H, Sullivan J M,

Erwin S C and Nadgorny B 2005 Phys. Status Solidi B 242 R67

[9] Arras E, Caliste D, Deutsch T, Lan¸con F and Pochet P 2011

Phys. Rev. B 83 174103

[10] Dau M T, Spiesser A, Le T G, Michez L A, Olive-Mendez S F, Le Thanh V, Petit M, Raimundo J M, Glachant A and Derrien J 2010 Thin Solid Films 518 S266

[11] Dau M T, Le Thanh V, Le T G, Spiesser A, Petit M, Michez L A and Daineche R 2011 Appl. Phys. Lett. 99 151908

[12] Le Thanh V, Bouchier D and Hincelin G 2000 J. Appl. Phys. 87 3700

[13] Spiesser A, Le Thanh V, Bertaina S and Michez L A 2011 Appl. Phys. Lett. 99 121904

[14] Abbes O, Xu F, Portavoce A, Girardeaux C, Hoummada K and Le Thanh V 2012 Defect Diffus. Forum 323–325 439

[15] Abbes O, Xu F, Portavoce A, Hoummada K, Le Thanh V and Girardeaux C 2011 Solid State Phenom. 172–174 579.

[16] Spiesser A, Virot F, Michez L A, Hayn R, Bertaina S, Favre L,

Petit P and Le Thanh V 2012 Phys. Rev. B 86 035211

[17] Gajdzik M, S¨urgers C, Kelemen M T and L¨ohneysen H 2000

J. Magn. Magn. Mater. 221 248

[18] Slipukhina I, Arras E, Mavropoulos P and Pochet P 2009

Appl. Phys. Lett. 94 192505

[19] Spiesser et al 2011 Phys. Rev. B 84 165203

[20] Spiesser A, Dau M T, Michez L A, Petit M, Coudreau C,

Glachant A and Le Thanh V 2012 Int. J. Nanotechnol 9 428

[21] S¨urgers C, Potzger K, Strache T, M¨oller W, Fischer G, Joshi N

and Löhneysen H 2008 Appl. Phys. Lett. 93 062503

[22] Yamada N 1990 J. Phys. Soc. Japan 59 273

[23] Matsui T, Fukushima T, Shigematsu M, Mabuchi H and

Morii K 1996 J. Alloys Compound 236 111

[24] Moison J M, Guille C, Houzay F, Barthe F and Van Rompay M

1989 Phys. Rev. B 40 6149

[25] Ohtani N, Molder S M, Xie M H, Zhang J and Joyce B A 1993

Surf. Sci. 284 305

[26] Zeng C, Zhang Z, Van Benthem K, Chisholm M F and

Weitering H H 2008 Phys. Rev. Lett. 100 066101

[27] Yoon D S, Roh J S, Lee S M and Baik H K 2003 Prog. Mater.

Sci. 48 275

[28] Becker J S and Gordon R G 2003 Appl. Phys. Lett. 82 2239

[29] Ting C Y 1984 Thin Solid Films 119 11

[30] Dau M T, Le Thanh V, Michez L A, Petit M, Le T G, Abbes O, Spiesser A and

Ranguis A 2012 New J. Phys. 14 103020